Airborne Doppler Lidar Measurements of Valley Flows in Complex Coastal Terrain

S. F. J. DE WEKKER

Department of Environmental Sciences, University of Virginia, Charlottesville, Virginia

K. S. GODWIN

Department of Environmental Sciences, University of Virginia, and Simpson Weather Associates, Charlottesville, Virginia

G. D. EMMITT AND S. GRECO

Simpson Weather Associates, Charlottesville, Virginia

(Manuscript received 21 December 2010, in final form 25 March 2012)

ABSTRACT

Three-dimensional winds obtained with an airborne Doppler lidar are used to investigate the spatial structure of topographically driven flows in complex coastal terrain in Southern California. The airborne Doppler lidar collected four hours of data between the surface and 3000 m MSL along a 40-km segment of the Salinas Valley during the afternoon of 12 November 2007. The airborne lidar measurements, obtained at horizontal and vertical resolutions of approximately 1500 and 50 m, respectively, reveal a detailed spatial structure of the atmospheric flows within the valley and their associated aerosol features. Clear skies prevailed on the flight day with northwesterly synoptic flows around 10 m s^{-1}. The data document a shallow sea breeze making a transition into an upvalley flow in the Salinas Valley that accelerates in the upvalley direction. Along with the acceleration of the upvalley wind, the lidar data indicate the presence of enhanced sinking motions. No return flows associated with the sea-breeze or upvalley flows are observed. While synoptic flows are aligned along the valley axis in the upvalley direction, lidar data indicate the presence of a northerly cross-valley flow around the height of the surrounding ridges. This flow intrudes into the valley atmosphere and induces, along with thermally driven slope flows on the sunlit valley sidewall, a cross-valley circulation that causes an asymmetric distribution of the aerosols. This study demonstrates the large potential of airborne Doppler lidar data in describing flows in complex terrain.

1. Introduction

The temporal evolution of thermally driven valley winds has been well investigated and is described in several reviews (e.g., Whiteman 1990). Valley flows occur when horizontal temperature differences along the valley floor produce a horizontal pressure gradient that results in upvalley flows during daytime and downvalley flows during nighttime (e.g., Wagner 1938; Whiteman 1990, 2000). The spatial structure of valley flows is often less understood, with flow structure affected by factors such as the presence of ambient synoptic-scale winds, tributary valleys, and adjacent oceans. These factors can make the spatial flow structure much more complicated. For example, in the case of an adjacent ocean, sea breezes can interact with valley flows to generate an extended sea breeze (e.g., Kondo 1990). In addition, synoptic flows can be subject to channeling into valleys (Whiteman 2000), and upvalley flows have been observed to accelerate along the valley floor (Rucker et al. 2008). Across the valley, flow heterogeneities have been observed that result from dynamical effects caused by bends in the valley (De Wekker et al. 2005; Weigel et al. 2006) and thermally driven cross-valley circulations (Bader and Whiteman 1989). Furthermore, ridgetop-level winds may modify the subsidence over the valley center during daytime and produce asymmetries in the cross-valley circulation (Zardi and Whiteman 2012). Documenting and investigating these and other complex spatial variabilities in wind structure caused by the interactions among valley flows, sea breezes, and ambient

Corresponding author address: Stephan F. J. De Wekker, University of Virginia, Dept. of Environmental Sciences, 291 McCormick Rd., P.O. Box 400123, Charlottesville, VA 22904-4123.
E-mail: dewekker@virginia.edu

DOI: 10.1175/JAMC-D-10-05034.1

flows is especially important for transport studies in which deviations from the mean wind structure can lead to large differences in dispersion of air pollution.

Studies in complex coastal terrain have mostly focused on the influence of coastal orography on the structure of the sea breeze (e.g., Banta et al. 1993; Banta 1995; Drobinski et al. 2006; Bastin et al. 2005, 2006). In the United States, this influence has been investigated intensively at Monterey Bay and the adjacent Salinas Valley in California, particularly during the Land and Sea Breeze Experiment (LASBEX) project (Intrieri et al. 1990). Ground-based Doppler lidar measurements during LASBEX indicated that the sea breeze consisted of two scales of flow in the vertical direction and in time: a shallow (a few hundred meters deep), strong ($\sim$6 m s^{-1}) sea breeze with a horizontal scale of 30–40 km starting between 0900 and 1000 LST and a weaker, deeper sea breeze with a horizontal scale of 100 km forming later in the day around noon (Banta et al. 1993). These two flows eventually merged into a well-blended layer of onshore flow about 1 km deep. Other investigators (e.g., Fosberg and Schroeder 1966; Johnson and O'Brien 1973) have also observed this dual structure of the sea breeze along the west coast of the United States. Darby et al. (2002) investigated the two scales of flow using two-dimensional model simulations and concluded that the land–water contrast is responsible for the shallow sea breeze and that the onset of deep slope flow associated with the coastal mountains is responsible for the weaker, deeper (up to $\sim$1500 m) onshore flow. The winds at the shore, below 1500 m, were most affected by the land–sea contrast and the coastal mountain range. Above 1500 m, winds at the shore were affected by the Sierra Nevada range located about 300 km away from the coastline. Slope flows generated by nearby sloping terrain affect the time of onset and the depth of the sea breeze (Darby et al. 2002). Also, whereas studies in which sea breezes have been investigated in isolation have clearly demonstrated the presence of return flows, these return flows have not been shown in the combined sea-breeze–valley wind system at Monterey Bay (Banta 1995).

An investigation of valley flows and the influence from sea breezes and ambient flows requires making three-dimensional observations of the spatial structure of flows in complex terrain at the local to mesoscale (1–100 km). Making these observations is an important but difficult challenge. Much progress has been made in obtaining observational information on the spatial wind structure for meteorological and environmental applications by Doppler lidars that were developed in the late 1960s [see Huffaker and Hardesty (1996) for a review]. Ground-based Doppler lidars have provided the research community with important new insights of thermally driven valley flows (Post and Neff 1986; Banta et al. 1999), sea breezes (Banta et al. 1993; Darby et al. 2002), and nocturnal jets (Banta et al. 2004), among other flow structures. Although a single ground-based scanning Doppler lidar obtains spatial wind structure information through the analysis of the measured radial velocity, the three-dimensional wind vector can only be obtained at one single location. To avoid this limitation, scanning Doppler lidars have also been mounted on airborne platforms since the late 1970s (Bilbro and Vaughan 1978; Bilbro et al. 1984; Bilbro and Emmitt 1984), enabling the documentation of atmospheric flows at high spatial resolution for larger spatial scales than those for ground-based Doppler lidars. Mountain–plain flows (Reitebuch et al. 2003; Weissmann et al. 2005) and sea breezes (Carroll 1989; Bastin et al. 2005, 2006; Drobinski et al. 2006) are among the studied flows using an airborne Doppler lidar. These previous studies investigated flow structure at a spatial resolution of about 10 km or larger, which is too coarse for studying across- and along-valley flow structure in many valleys. With increasing resolution of weather-forecasting and air-quality models, the documentation of flows at high spatial resolution ($\sim$1 km) becomes increasingly important so that these models can be evaluated and improved.

Over the past 10–15 years, the Integrated Program Office of the National Polar-Orbiting Operational Environmental Satellite System, with an eye to eventual deployment in space, has funded the development of an airborne Doppler lidar initially mounted in a U.S. Navy Twin Otter aircraft to conduct a variety of investigations. Since 2002, under the direction of Simpson Weather Associates and operated by the navy's Center for Interdisciplinary Remotely Piloted Research Studies, the Twin Otter Doppler wind lidar (TODWL) has flown more than 125 h of atmospheric missions. The TODWL has mostly obtained data at high spatial resolution over the Pacific Ocean and the complex coastal terrain of California, with the main purpose of retrieving winds over water surfaces and determining ocean-wave characteristics. A number of these flights were performed over the coastal mountains near Monterey Bay, however.

In this study, we use TODWL data to document and investigate the flow structure at high spatial resolution in the Salinas Valley of California and adjacent mountainous terrain. We focus our discussion on data collected during the TODWL flight on 12 November 2007, a fair-weather day with weak ambient winds. In contrast to previous measurements in the area, data were collected over a larger area and at much higher resolution (horizontal and vertical resolutions of $\sim$1500 and 50 m, respectively). Such measurements allow the investigation of interacting flows at multiple scales. Furthermore,

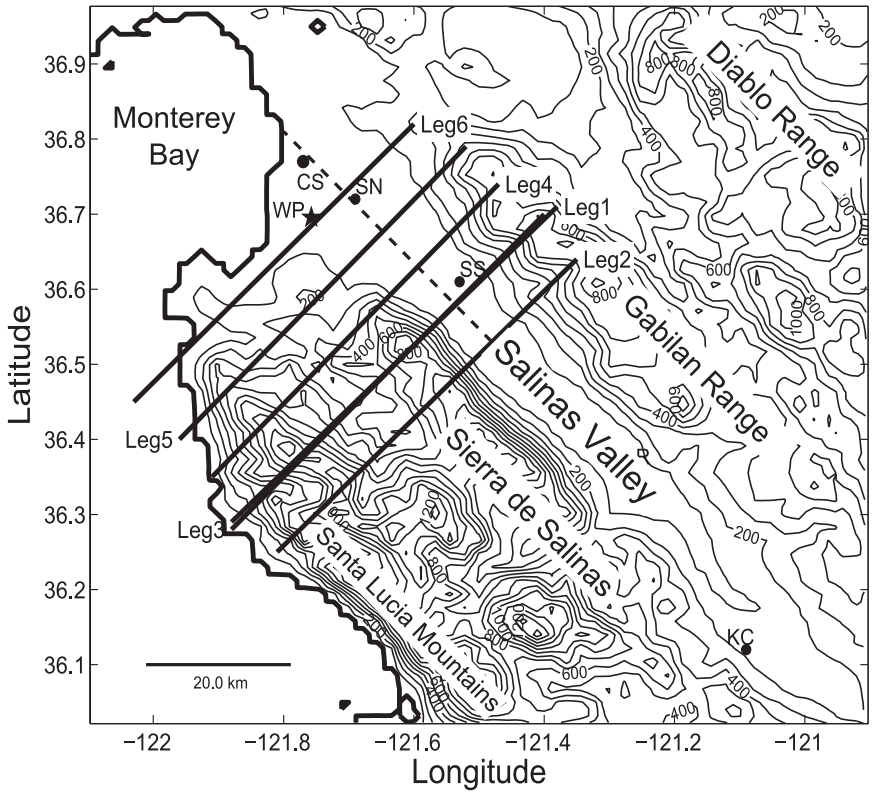

FIG. 1. Map of the investigation area including the Monterey Bay, Salinas Valley, and surrounding mountains. Contour lines show height in meters. The flight legs are shown with the solid black lines with the flight-leg number indicated at the starting point of each flight leg. The dashed line indicates the along-valley direction (~140° off north). The locations of the CIMIS surface stations (black dots) and wind profiler (black star), listed in Table 3, are also shown.

previous observational studies in the area have mostly been conducted from late spring to early autumn when thermally driven flows are prominent. Although surface heating in November is reduced relative to summer, winds in the Salinas Valley at this time can still be influenced by both the mountain-induced flows and the sea-breeze systems. A complex wind pattern can therefore be expected with potential additional influences of other mesoscale flows and synoptic background flows. We present some details of the topography of the investigation area and the collected data in section 2. In section 3, we present and discuss the observed wind and aerosol structure on 12 November 2007, followed by conclusions and outlook in section 4.

2. Data and data domain

All data shown in this study were collected in the complex coastal terrain near Monterey Bay. The investigation area consists of complex shoreline, a coastal region with several parallel mountain ranges oriented from north-northwest to south-southeast, and the interior valleys of California to the east (Fig. 1). The Salinas Valley is bounded by the Sierra de Salinas to the west and the Gabilan and Diablo Ranges to the east. The adjacent mountain ranges have a maximum elevation of about 1000 m MSL. The western sidewall of the Salinas Valley is more uniform and steeper than the eastern sidewall, which is characterized by the presence of many side canyons and tributary valleys. The Salinas Valley is about 20 km wide at its mouth and extends about 130 km to the southeast at an orientation of 140° from north. The valley floor is almost flat, with a height increase of about 160 m from Monterey Bay to King City, located 100 km southeast from Monterey Bay. Land use in the Salinas Valley is dominated by agriculture—in particular, irrigated crops. Details of the Twin Otter Doppler wind lidar data and other data collected on 12 November are presented next.

a. Twin Otter Doppler wind lidar data

The TODWL is a 2-μm coherent system built by Coherent Technologies, Inc. (now Lockheed Martin Coherent Technologies). Table 1 summarizes some of

TABLE 1. Characteristics of the TODWL system.

Wavelength	2 μm (eye safe)
Energy per pulse	2 mJ
Pulse length (temporal; spatial)	320 ns; 48 m (full width at half max)
Pulse repetition frequency	100 Hz (500-Hz max capability)
Data-processing range gate	96 m
Profile range gate resolution	50 m[a]
Line-of-sight measurement accuracy[b]	$\sim$0.2 m s^{-1}
Wind-component accuracy[c]	$<$0.5 m s^{-1}

[a] This range-gate resolution results in some photon sharing between adjacent data-processing gates.

[b] The value used in this table has been estimated assuming an accumulation of 100 shots at a fixed dwell angle and a ground-return-based calibration to account for aircraft motion.

[c] This is a value that is based on considerations using 12 radial velocities in a 20° off-nadir scan. The accuracy value is dependent upon the specific atmospheric conditions and various other factors.

the technical details of the lidar. With its side-door-mounted, biaxis scanner the beam can be adaptively directed in a variety of scan patterns, including conical, nadir stares, and flight-level stares. Thus, a defining capability of the TODWL is its ability to profile above, on, and below the flight level. The accuracies in Table 1 are estimates, because it is challenging to find truth datasets for the step-stare sampling pattern from a moving platform. We rely in large part on work by Frehlich (2001, 2004) and Frehlich and Sherman (2005) who developed much of the signal processing and error characterization for ground-based coherent Doppler lidar observations. The accuracies are dependent upon many factors such as aerosol distributions within the pulse length, wind turbulence within the illuminated volume of the accumulated pulses (for a single radial velocity estimate), aircraft motions, wind field characteristics, and signal-processing-related uncertainties (e.g., spectral resolution). As a consequence, there is no single accuracy value that applies to all situations. The accuracy of the horizontal and vertical wind components reported here are based upon data taken during the period and location of study and may change with sampling conditions.

To measure the wind velocity and wind direction with a Doppler lidar, conical scanning of the laser beam around the vertical axis is commonly used. Such a measurement method has traditionally been referred to in the Doppler radar community as the velocity azimuth display (VAD; Lhermitte and Atlas 1961; Browning and Wexler 1968). During the TODWL flights in the current study, 12-point step-stare scans were performed in which the azimuth angle changes in steps of 30°. The 12 radial velocities are used in the wind retrieval algorithm to produce an individual wind vector. The typical dwell time at each stare is about 1 s, during which 500 pulses are transmitted into the atmosphere. With the transition from one stare to another stare of about 1 s, the total time it takes to complete a full rotation of the scanner is about 20–30 s. The rotating lidar is projected 20° off nadir, and a dedicated global positioning system/inertial navigation system is used to correct for aircraft attitude. The ground speed of the aircraft is 50–60 m s^{-1} so that during that time a distance of about 1500 m is covered. In other words, a vertical profile of the horizontal and vertical wind component is obtained about every 1500 m. The selected vertical resolution (or, to be more accurate, grid spacing) of the wind profile is 50 m up to a height of about 2500 m, which is nominally 500 m below the aircraft altitude of 3000 m. The vertical resolution of a Doppler lidar measurement is dependent on the pulse length of 320 ns, which is, in the case of the TODWL, approximately 48 m long at its full width at half maximum. Because the raw data are processed using 96-m gates, there is an overlap of photon returns between sequential 50-m-resolution range gates. Note that the horizontal and vertical resolutions obtained by TODWL are higher than the resolution obtained in previous airborne Doppler lidar studies (e.g., Weissmann et al. 2005; horizontal and vertical resolution of 5 km and 100 m, respectively). These other studies had higher aircraft speeds and different scanning patterns. Unfortunately, winds below 300 m AGL are difficult to retrieve from airborne lidar since the ground return from the emitted lidar pulse intensifies and overwhelms the aerosol signal near the surface. Efforts to improve the retrieval of these winds are ongoing and involve a better identification of the aerosol signal. In some cases, these efforts have resulted in a retrieval of an extra 100 m (Godwin et al. 2012).

Doppler lidars not only provide the radial velocities but also the signal-to-noise ratio (SNR) for each range gate. Because the SNR is related to both the aerosol composition and concentrations, we can use the SNR as a first-order visualization of the spatial aerosol structure. The potential temperature and aerosol structure are often closely related. For example, in a convective boundary layer with vigorous mixing, one might expect a homogeneous distribution of aerosols with a sudden increase at the height of an elevated inversion where stability is large and mixing inhibited. As a consequence, the aerosol structure provides some guidance on the presence of distinct atmospheric layers (e.g., De Wekker et al. 2004).

A total of six cross-valley flight legs were flown across the Salinas Valley on 12 November 2007. The locations of the flight legs are illustrated in Fig. 1. Two of the legs

TABLE 2. Characteristics of the six flight legs flown on 12 November 2007.

Leg	No. conical scans	Mean profile separation (km)	Total distance (km)	Begin time (LST)	End time (LST)
1	45	1.48	66.73	1216	1231
2	38	1.58	59.95	1400	1410
3	50	1.31	65.54	1419	1434
4	50	1.28	64.11	1441	1451
5	58	1.08	62.86	1459	1514
6	44	1.32	58.28	1520	1530

TABLE 3. Name and location of the five surface weather stations from the CIMIS network and the 915-MHz radar wind profiler.

Station identifier	Station name	Lat	Lon	Elev (m MSL)	Distance from coastline (km)
CS	Castroville	36.77	−121.77	3	2.5
SN	Salinas North	36.72	−121.69	18	10.5
SS	Salinas South	36.61	−121.53	36	26.5
AR	Arroyo Seco	36.36	−121.29	70	58.5
KC	King City	36.12	−121.08	162	90.5
WP	Fort Ord	36.70	−121.76	48	4.5

(first and third) followed similar paths and were flown 2 h apart. Each of the legs covered a distance of up to about 60 km and were oriented in a northeast–southwest direction perpendicular to the orientation of the valley. The legs were separated by about 8 km in the along-valley direction. The flights took place between 1200 and 1530 LST. The start and end times of each flight leg are given in Table 2. During each leg, up to about 50 downward conical scans were performed.

b. Other data

Data from five surface stations and an operational wind profiler in the Salinas Valley/Monterey Bay area are used to describe the temporal changes in the wind. The surface stations are part of the California Irrigation Management Information System (CIMIS) network. The Castroville station is located closest to the coast line and the wind profiler location. The north and south Salinas stations are within the investigation area while Arroyo Seco and King City are located farther up the Salinas Valley (see Table 3 and Fig. 1). Data from the CIMIS network include temperature, winds, and net radiation at 1-h intervals. Vertical wind profiles at half-hourly interval were obtained from the Fort Ord 915-MHz boundary layer wind profiler, which is part of the coastal profiling network operated by the Naval Postgraduate School. The profiler is operated in two modes, resulting in vertical profiles with a resolution and range of approximately 50 m and 1 km in the fine mode and 200 m and 3 km in the coarse mode. The closest National Weather Service rawinsonde location is in Oakland, California, which is more than 100 km north of the investigation area. These data are of limited usefulness for the investigation of mesoscale flows in the Salinas Valley. In situ meteorological data on the Twin Otter aircraft were not recorded on 12 November.

3. Observed flows in and around the Salinas Valley

In this section, we will first describe the general atmospheric conditions on 12 November 2007, followed by a discussion of the data collected during the TODWL flight on that day.

a. General atmospheric conditions on 12 November 2007

Clear skies prevailed in the investigation area on 12 November 2007 with weak north-northwesterly synoptic flows of ~5–10 m s^{-1} at 850 hPa (Fig. 2; note that LST = UTC −8 h for the Salinas Valley). These weak synoptic flows promoted the development of thermally driven flows in the area. Data from all five surface stations show a shift from southeasterly (downvalley or offshore) to northwesterly (upvalley or onshore) flows around noon LST with hourly mean wind speeds at 2 m AGL of up to 5 m s^{-1} during the various TODWL flights between 1200 and 1530 LST (Fig. 3). The shift from downvalley to upvalley flows occurs latest (~noon LST) at King City, which is located farthest up the valley. In going from the northerly to the southerly stations, afternoon winds turn from westerly to northwesterly winds as the westerly sea breeze channels into the northwesterly aligned Salinas Valley. Maximum wind speeds increase in the upvalley direction. Average wind conditions for November for the 2003–07 time period indicate that the diurnal variability of wind and temperature on 12 November follows the climatological average (not shown). Associated with the turning of the wind from offshore to onshore, a decrease in temperature occurs at Castroville and Salinas North. Farther up in the Salinas Valley at Salinas South, this decrease in temperature occurs later in the afternoon around 1430 LST consistent with the propagation of a sea-breeze front at about 4 m s^{-1}. Note the increase in the diurnal temperature range up the valley, which is typical of valley atmospheres where valley volume decreases up the valley while heat input approximately remains the same (e.g., Whiteman 2000). Maximum temperatures range from 17°C at Castroville to 23°C at King City. Data from nearby buoys indicate a seawater temperature of ~14°C.

Data from the Fort Ord wind profiler provide detailed information on the temporal evolution of the vertical

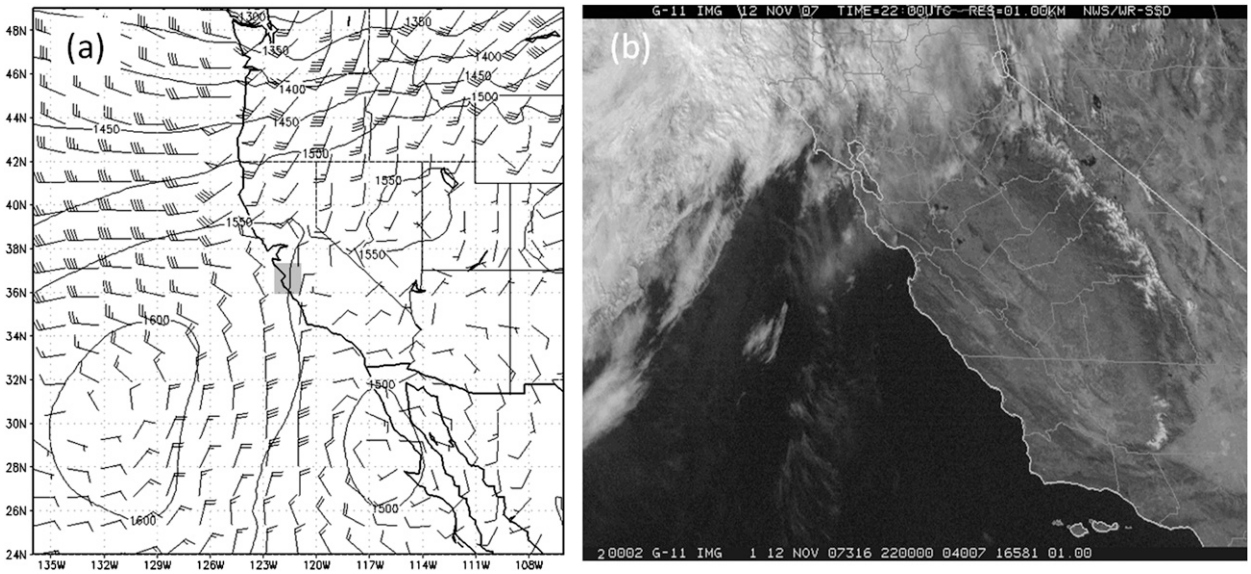

FIG. 2. (a) Geopotential height (m) and wind at 850 hPa at 2100 UTC 12 Nov 2007 (LST = UTC − 8 h). A full barb denotes 10 kt (1 kt ≈ 0.5 m s^{-1}). The area from Fig. 1 is indicated with the shaded box. (b) Corresponding Geostationary Operational Environmental Satellite image (visible channel) for 2200 UTC 12 Nov. Note that the scales in the two figures are different. The investigation area is approximately in the center of both figures.

wind structure near Monterey Bay (Fig. 4). Near the surface (below 300 m), southeasterly (offshore) winds of ~6–9 m s^{-1} prevail during the night and in the early morning up to about 0800 LST. Later in the morning, surface winds first turn to an easterly/northeasterly direction while decreasing in speed, followed by a change to stronger (up to 6 m s^{-1}) northwesterly winds in the afternoon. The turning from easterly to northeasterly flows in the morning up to about 600 m is likely due to thermally driven upslope flows initiated on the east-facing sidewalls of the coastal mountains. Westerly and northwesterly flows commence shortly after noon, indicating the onset of the sea breeze. At altitudes above 600 m, winds gradually turn to the geostrophic northwesterly winds. From midmorning onward, winds are weaker than 10 m s^{-1} up to a height of about 2000 m except for a couple of hours in the afternoon when a distinct wind speed maximum of just over 10 m s^{-1} occurs at heights around 1300 m. The timing of this wind speed maximum coincides with the

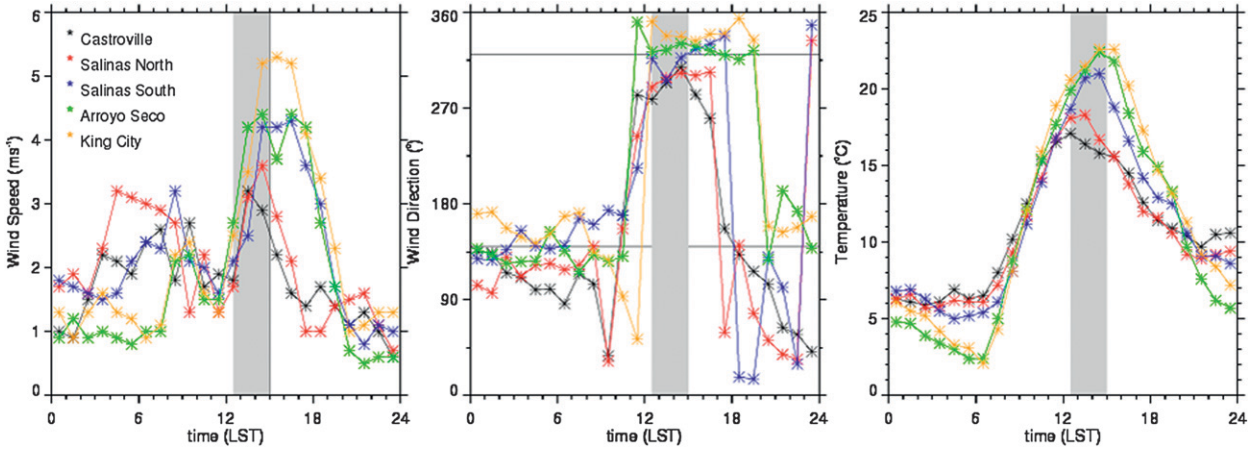

FIG. 3. Diurnal evolution of (a) wind speed, (b) wind direction, and (c) temperature at the five CIMIS network surface stations on 12 Nov 2007. Wind and temperature are measured at 2 and 1.5 m AGL, respectively. The gray rectangle in the figures denotes the approximate time period during which the flights took place; the horizontal lines in (b) denote the upvalley wind direction (320°) and downvalley wind direction (140°).

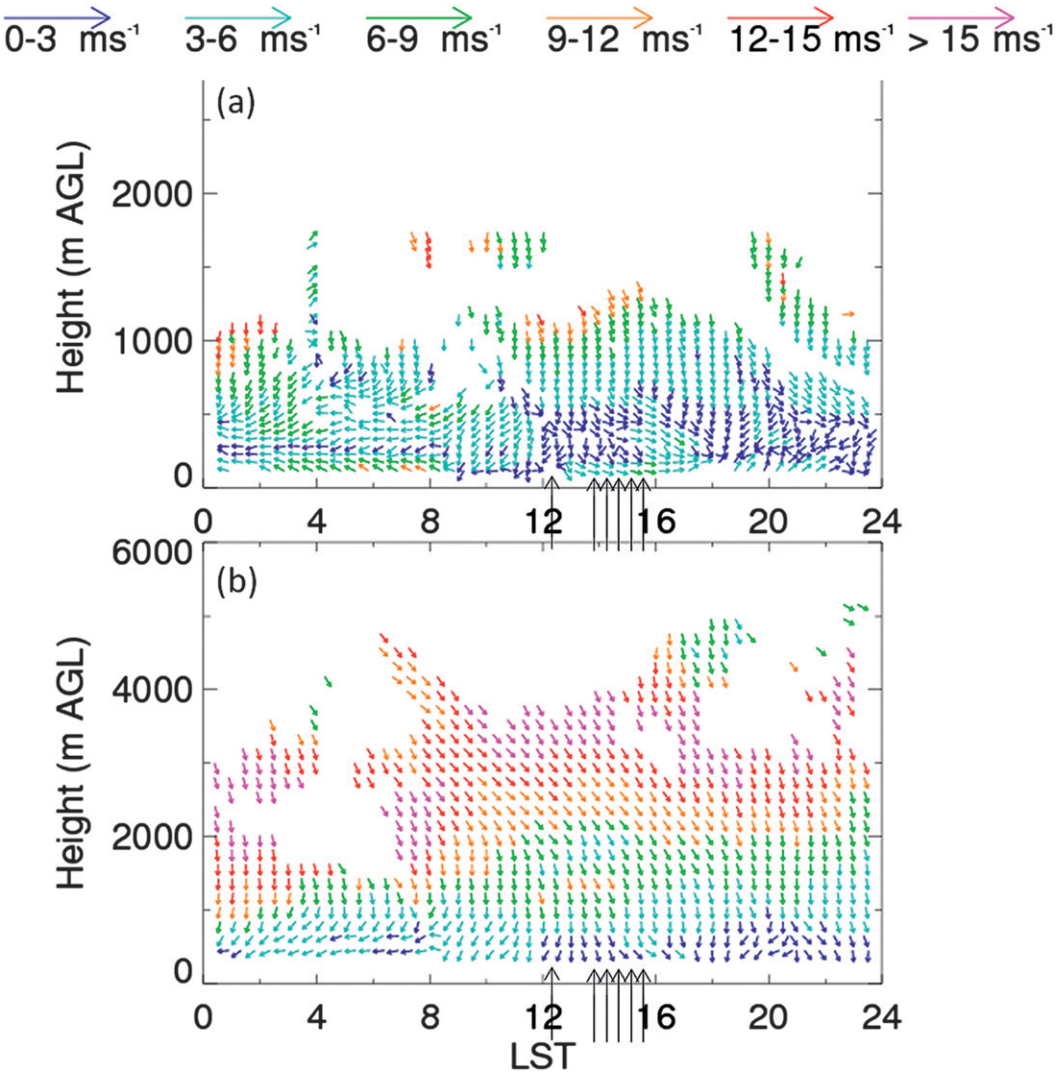

FIG. 4. Time–height cross section of wind speed and direction at Fort Ord from (a) coarse-mode and (b) fine-mode wind profiler measurements. The vertical arrows indicate the times of TODWL flight legs 1–6.

timing of the TODWL flight legs, indicated by the vertical arrows in Fig. 4.

While this wind speed maximum appears to be of short duration, its spatial extent is large and obvious from the TODWL data, as will be discussed in the next section. The wind speed maximum can be seen more clearly in the vertical profiles in Fig. 5, which also shows that the wind direction is persistently from the northwest and that the wind speed maximum disappears later in the afternoon. The spatial extent of the wind speed maximum of just over 10 m s^{-1} between ~1000 and 1500 m is unclear from the vertical profile data alone. Figure 5 also shows a vertical profile of the Doppler lidar–derived horizontal wind speed and direction and the vertical wind speed at 1529 LST at about 8.5 km from the Fort Ord wind profiler. The lidar and wind profiler winds compare well and show that the TODWL data capture the wind speed maximum well and at higher vertical resolution than do the wind profiler data. Although there is generally a good agreement between the radar wind profiler and airborne Doppler lidar–derived winds, it is understood that the averaging time and the sampled volume are different for the two observing systems. This could explain, for example, the worse agreement with the 1600 LST radar profiler data. The strength of the TODWL data is in capturing the wind structure at high spatial resolution, which we will discuss in the next section. Note that, directly above the shallow westerly sea breeze layer of a few hundred meters, winds are weak (<2 m s^{-1}) and from northerly directions. Boundary layer heights determined from the wind profiler data using the SNR indicate a maximum height of

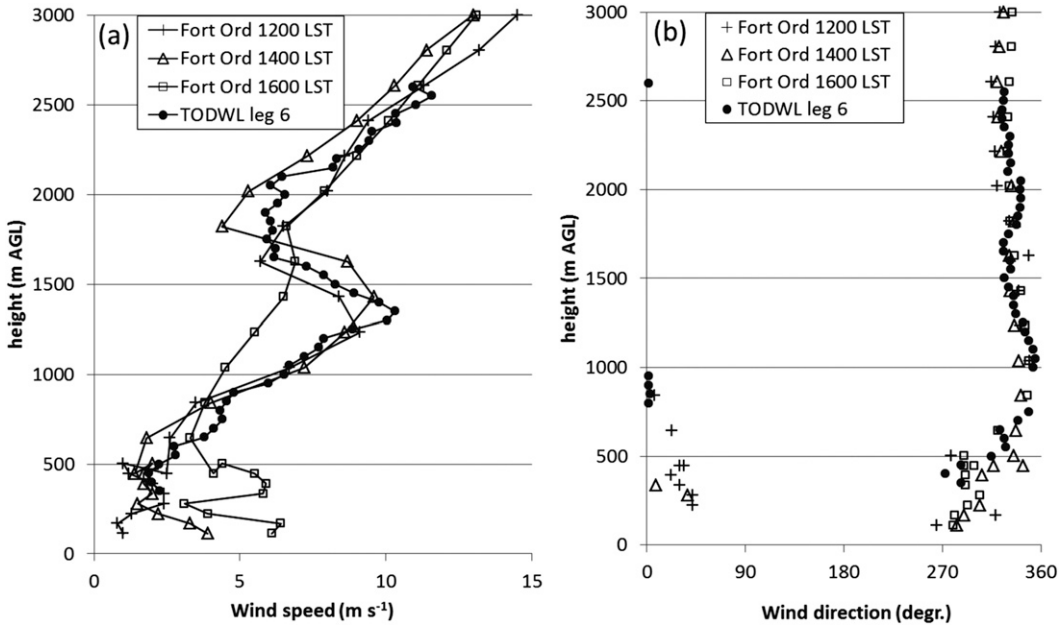

FIG. 5. Vertical profiles of (a) horizontal wind speed and (b) wind direction from wind profiler measurements at Fort Ord at 1200, 1400, and 1600 LST and from TODWL near the location of Fort Ord (36.70°N, −121.76°W) at 1529 LST during flight leg 6. Wind profiler measurements are from the fine mode under 500 m and from the coarse mode above 500 m.

~600 m MSL. The onset of the sea breeze is much delayed relative to previous summertime observations when the onset ranged from 0830 to 1030 LST (Fagan 1988; Banta et al. 1993). In November, the land heats up more slowly and less intensely and the sea-breeze onset is therefore expected to be delayed.

b. Doppler lidar data results

We will first discuss the spatial variability of the wind and aerosol structure in the entire flight area, followed by a detailed analysis of the flows in and at the exit of the Salinas Valley. The temporal evolution along the Salinas Valley cross section that was covered by two flight legs (1 and 3) made 2 h apart is also discussed. This entire flight took place in the afternoon, shortly after the surface winds changed from an offshore/downvalley direction to an onshore/upvalley direction.

1) SPATIAL WIND STRUCTURE IN THE ENTIRE FLIGHT AREA

Figure 6 shows the spatial structure of the horizontal winds and the SNR for flight legs 2–6. The horizontal wind vectors are only shown every 200 m in the vertical direction. Three layers are clearly present, each of which has an increasing SNR going from the top to the bottom layer. The approximate boundaries of these three layers are indicated in Fig. 6b by horizontal dotted lines. A layer with the lowest SNR and northwesterly winds of larger than 10 m s^{-1} is present above ~2000 m. Winds in this layer, which we identify as the ''free atmosphere'' (indicated as layer 1 in Fig. 6b) and which represents the synoptic flow, are spatially homogeneous across the coastal mountainous terrain. The transition to synoptic flows above 2000 m was also seen in Figs. 4 and 5.

Up to a height of ~1300 m, a layer with the largest SNR is found (indicated as layer 3 in Fig. 6b). This surface-based layer becomes somewhat shallower in the southernmost legs with a more heterogeneous structure as the variability in terrain height increases. Furthermore, there is a tendency for a deeper and more concentrated aerosol layer over the eastern sidewalls of the Salinas Valley as seen in Figs. 6f, 6h, and 6j. A possible explanation for this behavior of the aerosol layer is provided section 3b(2). Weak flows (<6 m s^{-1}) dominate in this layer with increasing speeds up the valley (cf. wind speeds in Salinas Valley among Figs. 6c, 6e, and 6g).

An interfacial layer is present between the surface-based layer and the free atmosphere (indicated as layer 2 in Fig. 6b). Winds in this layer and in the surface-based layer are generally between 4 and 10 m s^{-1}. Note, however, the larger wind speeds at the interface of these layers at about 1300 m where the sudden decrease in SNR indicates a change in stability. Furthermore, there is a tendency for stronger winds in this interfacial layer closer to the coastline than farther inland contrary to the flows near the surface.

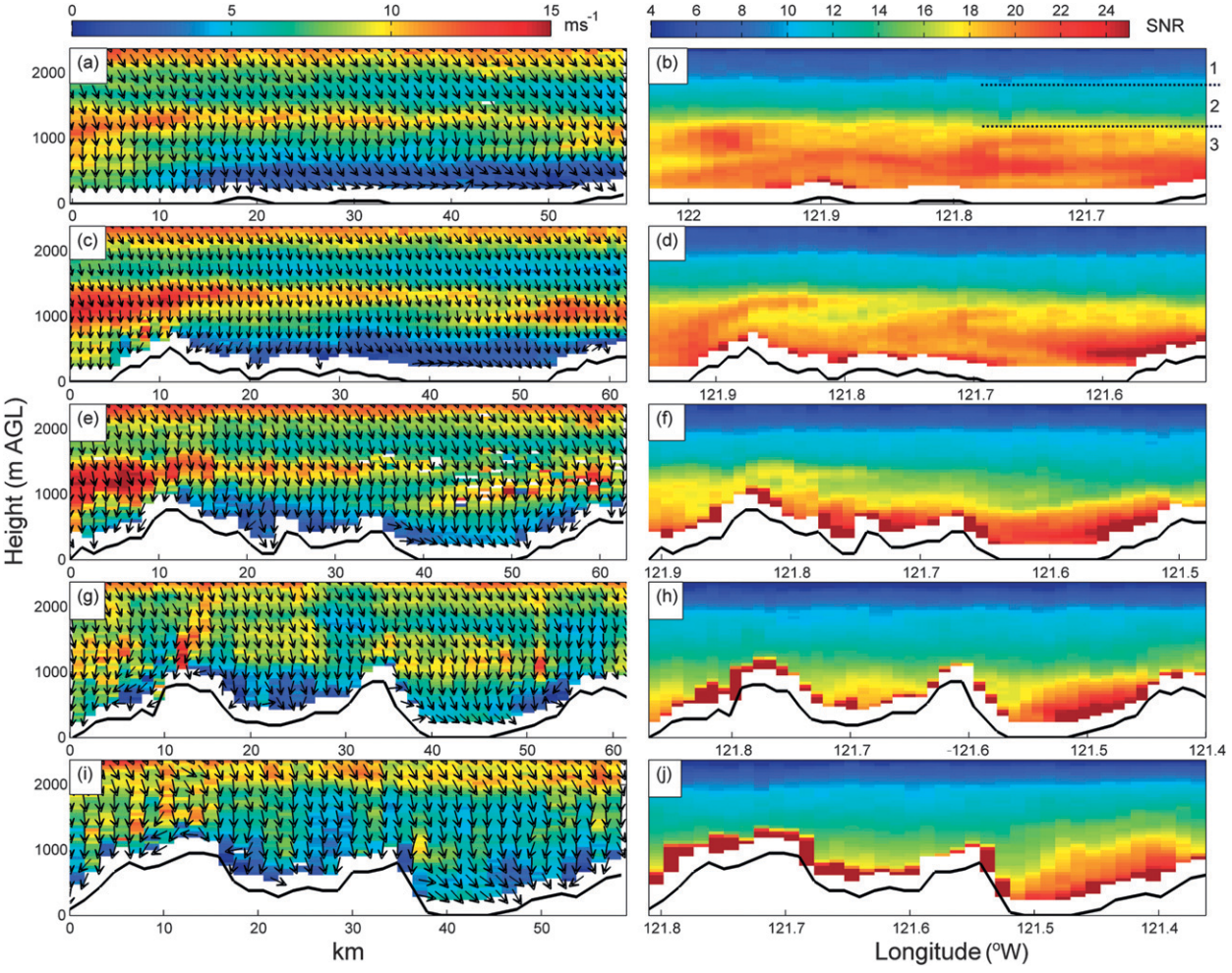

FIG. 6. Vertical cross section of the TODWL-derived (left) horizontal wind and (right) SNR for (a), (b) flight leg 6, (c), (d) flight leg 5, (e), (f) flight leg 4, (g), (h) flight leg 3, and (i), (j) flight leg 2. Wind vectors are only shown at every 200-m height level. The approximate boundaries of three layers with different SNR (layers 1, 2, and 3) are indicated in (b) by horizontal dotted lines.

It is well known that close to the coastline the northwesterly flow is enhanced by coastal baroclinicity and often results in a coastal jet near the strong inversion capping the marine boundary layer (Zemba and Friehe 1987; Beardsley et al. 1987). Operational model output from the Coupled Ocean–Atmosphere Mesoscale Prediction System (COAMPS) model at 3-km grid spacing does not clearly show evidence of a strong temperature inversion and/or a wind speed maximum. On the basis of previous studies, however, it is expected that a strong temperature inversion between 1000 and 1500 m is present coincident with the observed wind speed maxima. An indication of the presence of a strong temperature inversion is provided by in situ flight data collected in the evening of 11 November 2007. Because of the diurnal variability of the coastal baroclinicity, the coastal jet has a diurnal cycle, with the most pronounced and strongest jet close to the coast during mid-to-late afternoon (Cui et al. 1998). The relative maximum of the winds in a layer between 1000 and 1500 m that is particularly evident in the northwestern part of the flight domain could be the result of this coastal jet. We also notice that in legs 4–6 the core of this wind maximum extends to the east and corresponds to the wind maximum found at ~1300 m in the wind profiler data at Fort Ord (Figs. 3 and 4). The TODWL data therefore indicate the presence of a coastal wind maximum that affects the wind fields not only over the water but also farther inland. Note that the height of a coastal wind maximum has usually been observed in previous investigations to be closer to the surface at around 500 m. Those observations are made in the summertime when subsidence associated with the Pacific high is stronger and suppresses the depth of the marine boundary layer

relative to the late-autumn period in which our observations were made.

Besides an increase in the winds above the western part of the Salinas Valley that appears to be an extension of the coastal jet, there also is an apparent wind maximum at and above ridge height in the eastern part of the valley, which again is most obvious in the northernmost legs. In the next section, we will discuss in more detail these and other flow features observed in the Salinas Valley.

2) SPATIAL WIND STRUCTURE IN THE SALINAS VALLEY

The acceleration of the along-valley flow in the Salinas Valley and the wind maximum in the eastern part of the domain identified previously become more obvious when considering a horizontal cross section of the flows at various heights as shown in Fig. 7. Decreasing in elevation from 2000 to 1000 m MSL (Figs. 7a–c), the approximate maximum height of the surrounding ridges, winds increase in strength and change toward northerly and even toward more easterly directions. These northerly and easterly flows are also apparent at lower elevations (800 and 600 m) while at 400 m MSL the flows are clearly aligned along the valley axis. These along-valley flows increase in speed with distance upvalley. Also note the relative wind maxima in the western part of the valley at 1500 m (Fig. 7b) and in the eastern part of the valley at 1000 m (Fig. 7c) that were mentioned in the previous section.

A closer look at the vertical profiles of wind speed and direction (Fig. 8) reveals a similarity of the wind structure among the different locations along the valley with relative wind speed minima and maxima at ~500 and 1000–1500 m MSL, respectively. Below 500 m MSL, wind speeds increase, and a wind speed maximum is anticipated at a few hundred meters above the surface. Wind speeds at 300 m AGL correspond well to the wind speed measurements at the CIMIS surface stations (Fig. 3). Ongoing efforts to improve the retrieval of airborne Doppler lidar winds below 300 m AGL reveal a further increase of the wind speeds near the surface for this case study (Godwin et al. 2012). Note that, below 500 m MSL, winds near the coast are westerly (onshore), indicating a clear influence from the sea breeze.

Previous studies of the sea breeze at Monterey Bay have indicated similar depths of the sea breeze (on the order of a few hundred meters) and a similar structure including the absence of a return flow. Return flows related to the sea-breeze circulation are commonly observed over flat terrain but have not been observed in isolation in the Monterey Bay area in this and in previous studies (Intrieri et al. 1990; Banta et al. 1993). Possible reasons for the absence of a return circulation are the strong synoptic forcing and complex inland topography that cause the return flow to be either incorporated into the slope–valley wind system or absorbed into the deep inland boundary layer (Banta et al. 1993). Although return flows are absent, a clear minimum in the onshore wind component is present between ~300 and 500 m (Figs. 4 and 8) where a return flow may be expected (e.g., Simpson 1994). The height of the wind speed minimum also corresponds to the typical height of the internal boundary layer along the coast.

In the upvalley direction, the wind speed minima and maxima become less distinct. Valley averaged winds between 350 and 500 m MSL increase with distance up the valley from 1 to 5 m s^{-1} (Fig. 9a). This increase is still present for winds averaged between 550 and 700 m (Fig. 9b) but disappears above 750 m (Fig. 9c). The vertical wind shear below 1000 m MSL is thus strongest near the coast and at the valley exit. In leg 2, the southernmost leg, the mean vertical wind shear (in speed and direction) and the wind speed maximum at ~1000 m MSL are smallest, which suggests increased vertical mixing within the valley atmosphere. While wind speed variability decreases in the vertical direction with increasing distance up the valley, the wind speed variability increases across the valley (Fig. 8), especially below ridgetop level, with the largest wind speeds usually occurring near the center of the valley (Fig. 7).

An acceleration of the along-valley flow has been observed in other valleys (e.g., Rucker et al. 2008; Whiteman 2000). Such an acceleration is counterintuitive because one might expect a loss of valley airmass through the tributary valleys and side canyons (Zardi and Whiteman 2012). An acceleration is normally attributed to the increase of the along-valley pressure gradient caused by stronger warming of the valley atmosphere in the upvalley direction. Dynamic channeling of the sea breeze could be another reason for the wind speed increase in the Salinas Valley. As the valley becomes narrower in the upvalley direction, as observed in many valleys including the Salinas Valley, both the warming and dynamical channeling are enhanced, resulting in a wind speed increase.

The along-valley flow divergence should lead to sinking motions in the valley. The vertical wind speeds from the Doppler lidar (Figs. 9d–f) suggest that this is indeed the case, with maximum valley-averaged sinking motions of about 0.2 m s^{-1} in flight leg 4. This flight leg is in that part of the along-valley segment where the strongest acceleration in wind speed took place (see also Fig. 7). An estimation of the vertical wind speed needed to maintain mass conservation, if one assumes that the observed flow divergence [$\Delta u/\Delta x = 4$ m s^{-1} (14.5 km)$^{-1}$]

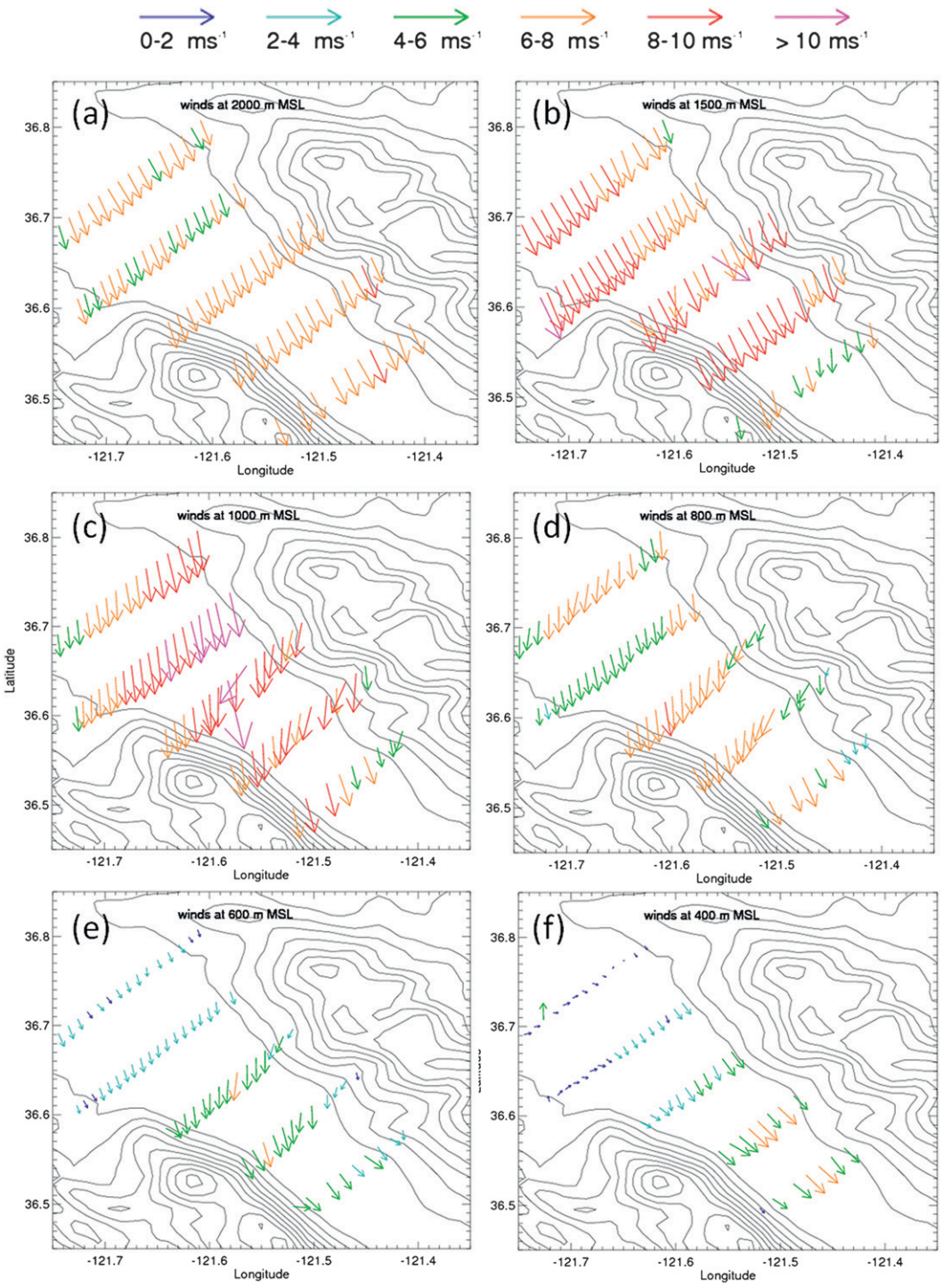

FIG. 7. Horizontal cross sections of the TODWL-derived winds over the Salinas Valley at (a) 2000, (b) 1500, (c) 1000, (d) 800, (e) 600, and (f) 400 MSL.

takes place over a depth of 500 m, results in a value of about 0.1 m s^{-1}. Of interest is that, although the acceleration of the along-valley flow decreases with height (cf. Figs. 9a–c), sinking motions are still relatively large for flight leg 4 relative to the other flight legs in all height intervals (Figs. 9d–f). A detailed analysis of the corrections that are made to the raw data to account for aircraft motion and attitude revealed no apparent bias that

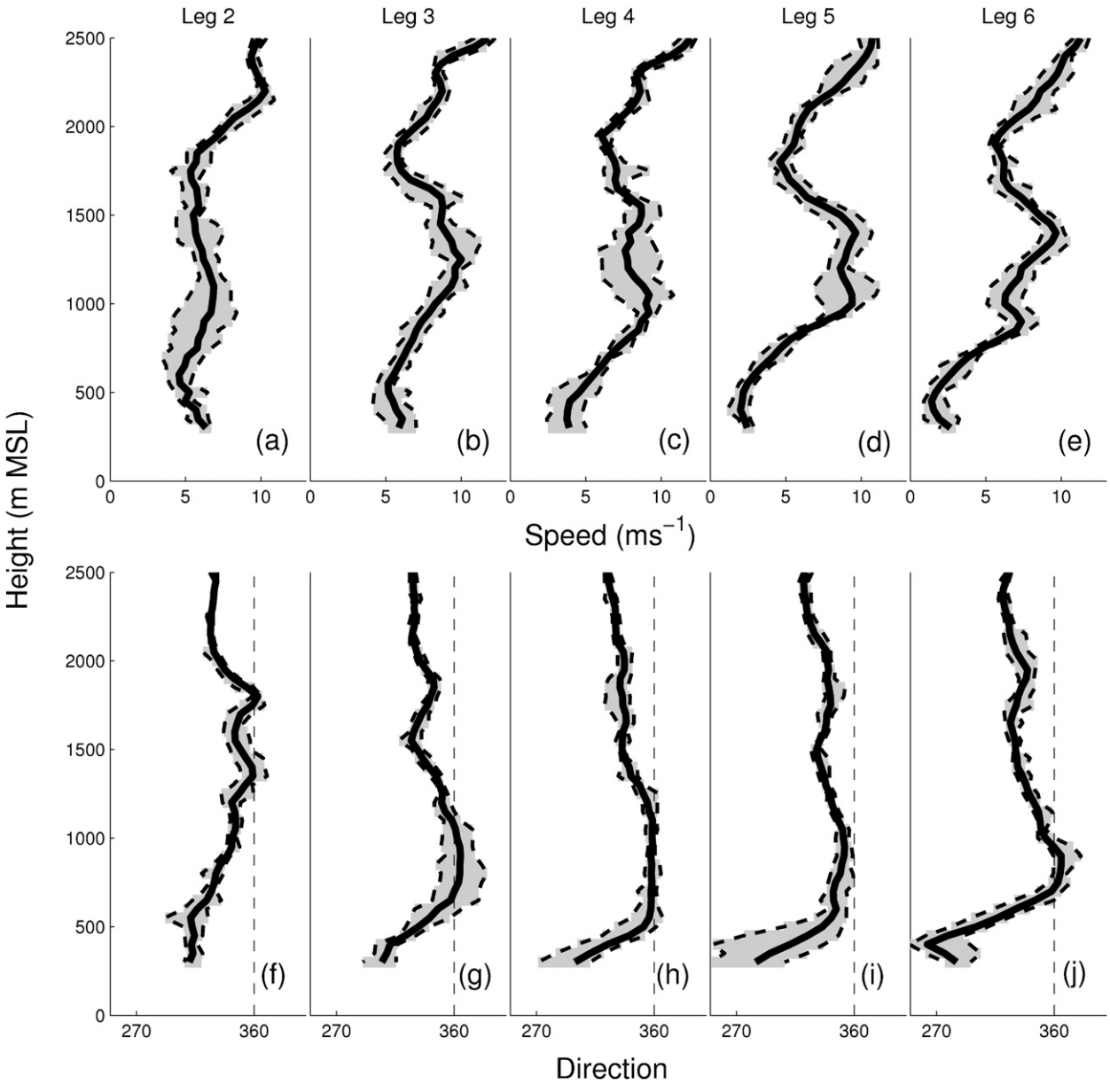

FIG. 8. Vertical profiles of TODWL-derived (a)–(e) wind speed and (f)–(j) direction averaged over the flat valley-floor section in the Salinas Valley for flight legs 2–6, as labeled. The gray shading bounded by the dashed lines indicates the range of wind speed and direction among the profiles.

could have caused this particular behavior for flight leg 4. Although the magnitude of this sinking motion is comparable to the uncertainty indicated in Table 1, the spatial coherence of the individual estimates shown in Fig. 9 supports the claim that there is organized subsidence to meet the mass divergence within the valley. As was stated in section 2, calculation of the wind components using the VAD algorithm relies on the assumption of horizontally homogeneous flow. An analysis of the effect of a divergence of the flow in the scanned volume on the wind retrieval using the VAD algorithm revealed that an acceleration of the observed magnitude could result in an apparent sinking motion of about 0.05 m s^{-1}. The TODWL-derived vertical velocity estimates, however, are larger than this value. We furthermore observed in the aerosol structure of leg 4 (Fig. 6f) a decreased height of the aerosol layer top around 1000 m relative to the adjacent flight legs indicating enhanced sinking motions over the Salinas Valley along leg 4. Possible reasons for enhanced sinking motions along

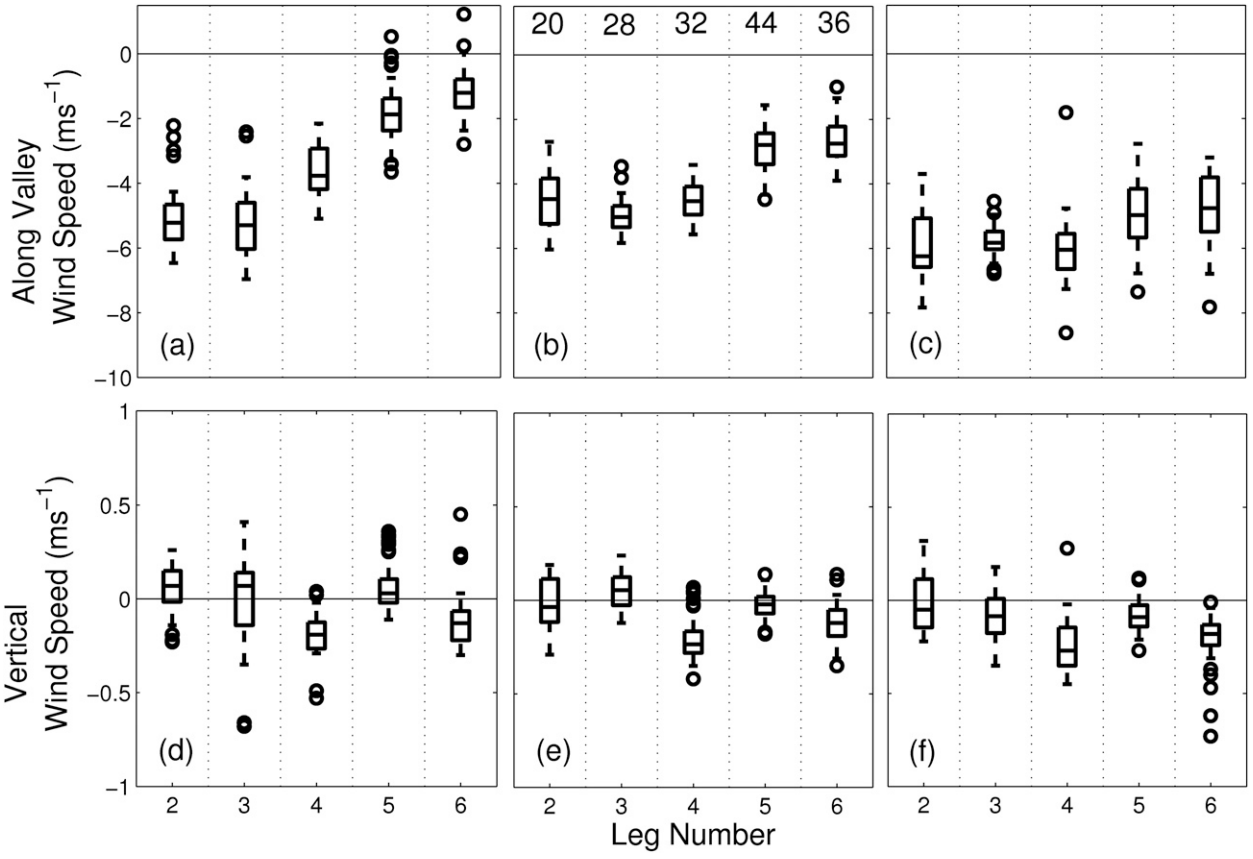

FIG. 9. Box-and-whisker plots of the (top) along-valley and (bottom) vertical wind speed at heights between (a), (d) 350 and 500 m; (b), (e) 550 and 700 m; and (c), (f) 750 and 900 m. Only wind data obtained over the flat Salinas Valley floor are used. The box encloses the interquartile range (25th–75th percentiles), and the whiskers extend out to the 12.5th and 87.5th percentiles. Open circles denote outliers. The number above each box in (b) is the number of data points used for the calculation of the statistics for a particular leg. Negative vertical wind speeds denote sinking motions.

a particular valley segment in addition to an along-valley flow divergence include a removal of airmass by upslope flows and flow diversion into the side canyons and tributary valleys. It is not clear why this would be more prominent along flight leg 4 than along the other legs within the Salinas Valley. Missing lidar data below 300 m AGL unfortunately do not allow us to investigate this further.

Another aspect of the flow that was noted before (and was seen in Figs. 6, 7, and 8) and deserves some attention is the wind speed maximum above the eastern part of the Salinas Valley just above 1000 m MSL, particularly in leg 5. This maximum can partly be explained by a jetlike structure in the cross-valley component of the wind as shown in Fig. 10. The jetlike structure is apparent across the entire valley, however, and not just on the eastern part of the valley. It is interesting that, despite the approximate alignment of the synoptic flows along the valley, such a prominent cross-valley wind structure is observed. The jetlike structure is present in all legs but becomes less distinct in the southernmost leg (leg 2). The cross-valley winds also appear to intrude at lower elevations in the Salinas Valley along flight legs 3 and 4. With a near surface (300–600 m MSL) across-valley wind component having the opposite direction, there is some indication of a cross-valley circulation in legs 2–4. The weaker easterly cross-valley component and stronger westerly cross-valley component near the surface in flight leg 2 relative to the other legs cause aerosols in flight leg 2 to appear concentrated on the eastern part of the Salinas Valley as shown in Fig. 6j. Convection and upslope flows on the heated eastern sidewall probably also play a factor. As noted before, the current inability of retrieving winds from Doppler lidar data below 300 m AGL does not allow an investigation of upslope flows.

The origin of the cross-valley winds is unclear at this point. Because of the presence of these winds in all flight legs and at elevations above the surrounding mountains, it appears that the flows are not just occurring on a local scale. Local-scale effects such as those caused by the

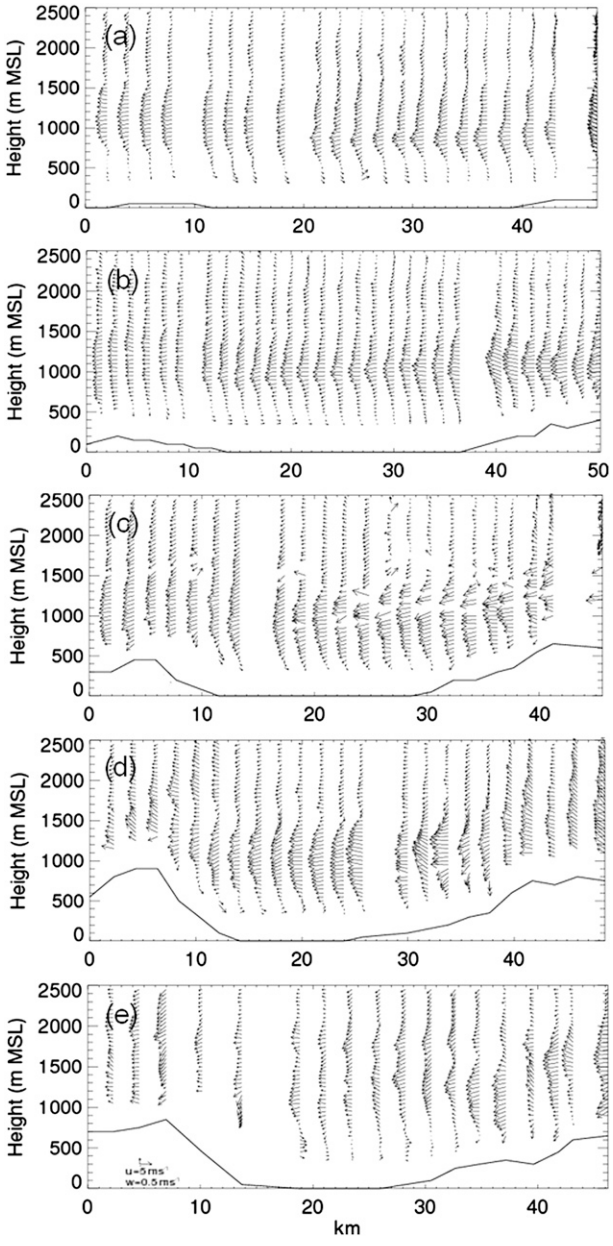

FIG. 10. Cross-valley wind component of the wind for flight legs (a) 6, (b) 5, (c) 4, (d) 3, and (e) 2. The cross-valley direction is defined as being perpendicular to the dashed line in Fig. 1. Only a subsection of the lidar cross section in Fig. 6 is shown.

aforementioned return flows associated with upslope and upcanyon winds along the eastern sidewall cannot be excluded, however. Another possibility includes a dynamical effect related to the specific shape of the valley sidewall and particularly at its exit (e.g., the pass toward San Joaquin Valley). These types of effects have been observed in smaller-scale valleys (Weigel et al. 2006). Previous studies (e.g., Darby et al. 2002) have indicated the influence of the Sierra Nevada on flows observed over the investigation area. During daytime, however, the effect would be a stronger westerly component of the flow, not an easterly component.

Two identical flight legs that were flown at approximately 1200 and 1400 LST allow an investigation of the temporal wind and SNR changes in the Salinas Valley. The first flight leg on 12 November took place shortly after a wind reversal at the surface from downvalley to upvalley direction (Fig. 3). Upvalley flows are present over the entire depth of the valley (Fig. 11a). In comparing leg 1 with leg 3, it is seen that valley-averaged winds have increased in speed from ~4 to 7 m s^{-1}. The maximum in the cross-valley wind component that was evident in Fig. 10 was also present during flight leg 1 but at altitudes that were about 500 m higher than during flight leg 3 (not shown). Both at 1200 and 1400 LST, winds are generally weakest in the eastern part of the valley atmosphere. If we assume that upslope flows are present in the lowest 300 m AGL over the sunlit slope, these flows could interact with the upvalley flows and reduce the wind speed. Some evidence of the presence of upslope flows is given by the asymmetric distribution of SNR, with higher SNR over the heated eastern sidewall at both times.

4. Conclusions and outlook

An airborne Doppler lidar was operated in the Salinas Valley and surrounding mountains as part of a field experiment in November of 2007. The major goal of this experiment was related to the support of the development of a spaceborne Doppler lidar, but the flights also provided detailed information on the complex spatial structure of afternoon flows in the coastal mountains of California.

The Doppler lidar, flown at an altitude of 3 km MSL and operating in a 12-point, 20° off-nadir step-stare conical-scanning mode, generated datasets from which horizontal and vertical velocities were derived with a horizontal resolution of 1500 m, a vertical resolution of 50 m, and an estimated accuracy of the wind components of <0.5 m s^{-1}. The mapping of aerosol layers and visualization of organized aerosol-laden structures yielded further information on flow stratification and dynamic processes.

To begin the mining of the Doppler lidar datasets, data from a flight on 12 November 2007 were used to develop methods of analyses and interpretive skills for a relatively new perspective on spatial wind structure in a valley. A thermally driven sea-breeze and upvalley flow developed around noon on this clear day on which northwesterly synoptic flows prevailed. The sea-breeze onset at noon is delayed by ~3 h relative what was

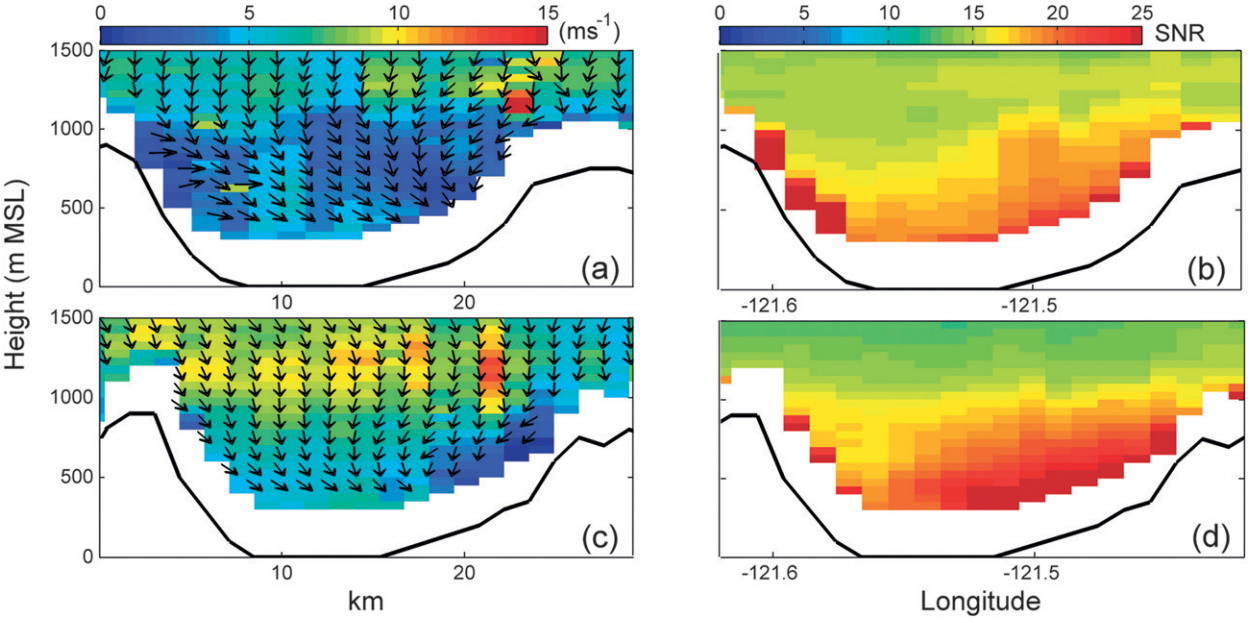

FIG. 11. Vertical cross section of the TODWL-derived (left) wind and (right) SNR for flight legs (a), (b) 1 and (c), (d) 3 at identical locations but showing flows that are 2 h apart from each other (~1200 vs ~1400 LST).

observed in previous studies in the area that were mostly conducted in summer. The sea breeze started as a westerly flow near the coast and turned into northwesterly upvalley flows in the Salinas Valley, increasing in speed from 2 to 6 m s^{-1} and in depth from ~400 to 600 m. Consistent with previous studies, no return flow was observed in the Salinas Valley. Although the winds were predominantly from northwesterly directions, a cross-valley component of the wind with a jetlike structure was present at heights between 1000 and 1500 m MSL and mostly on the eastern side of the valley. The origin of this cross-valley flow and its interaction with the upvalley flow within the Salinas Valley remain unclear. Another distinct wind maximum was found between 1000 and 1500 m MSL in the western part of the Salinas Valley. This wind maximum appears as an easterly extension of the wind maximum that was observed over the coastal waters.

The acceleration of the along-valley flow resulted in estimated vertical sinking motions on the order of 0.2 m s^{-1}, a value derived from both mass continuity considerations and the Doppler lidar data. Furthermore, while the vertical wind shear decreased in the upvalley direction the horizontal wind shear increased, with some indication of the presence of a cross-valley circulation. These processes resulted in an asymmetric distribution of the Doppler lidar–mapped aerosols across the Salinas Valley, with an elevated concentration of aerosols over the eastern sidewall.

In summary, as detailed by the Doppler lidar, the general picture of the flows in the Salinas Valley consists of a sea breeze making a transition into an upvalley flow that accelerates in the upvalley direction. Influences from synoptic flows, coastal jets, cross-valley flows, and slope flows cause a large spatial variability in the upvalley flow with wind speed maxima observed at and above ridgetop level and sinking motions within the valley. Although certain aspects of the flow features in the Salinas Valley have been observed in other valleys before—such as a transition from sea breeze to upvalley flow, an acceleration of the upvalley flow, and the presence of cross-valley flows—the detailed measurements of the three-dimensional winds provided by the Doppler lidar are unprecedented and provide information on flows from the local scale to the synoptic scale.

It is important to emphasize that the insight gained from airborne Doppler lidar is greater when coordinated with ground-based instrumentation to characterize meteorological conditions more completely and to reduce uncertainties in the interpretation of the airborne lidar data. A radar wind profiler located near Monterey Bay and a network of surface stations along the Salinas Valley provided the temporal information that aided the interpretation of the Doppler lidar data. An investigation of the stability structure and its role in the observed flows and aerosol structure was hampered by the lack of temperature-structure data and observations along the valley sidewalls. Because winds could not be faithfully retrieved from Doppler lidar below 300 m AGL, an investigation of the sea-breeze and upvalley wind maxima that occur in this layer and the upslope

flows over the sidewalls was not possible. Efforts are ongoing to improve the retrieval of winds in this layer near the surface (Godwin et al. 2012).

This paper demonstrated the ability of airborne Doppler lidar data to produce a detailed and comprehensive three-dimensional picture of atmospheric features and structure. The measurements allow an investigation of the integrated effects of multiscale flows on atmospheric transport and provide an important dataset for the evaluation of numerical models. This evaluation and the investigation of underlying processes explaining the observed flows will be performed with a mesoscale numerical model in a separate paper. Such an investigation will hopefully clarify the mechanisms underlying the various wind maxima in and above the Salinas Valley, the along-valley acceleration of the winds, the sinking motions, and the asymmetric aerosol structure. Future flight and scanning strategies in complex terrain should focus on collecting data in regions with large model uncertainty and/or in regions such as the slope boundary layer that are keys to understanding processes in complex terrain.

Because of recent developments in electronics at eye-safe wavelengths and in reducing costs of off-the-shelf components, it is expected that more airborne Doppler lidar systems will become available in the near future. Lighter-weight hardware components will also facilitate the mounting of Doppler lidar systems on aircraft with smaller payload, resulting in cheaper and therefore potentially more frequent and widespread operations. Research on the processing and interpretation of airborne Doppler lidar data and the combined use of the data with numerical model output is therefore important.

Acknowledgments. This research was supported by Grants W911NF0910076 from the Army Research Office and N000141110709 and N000141110450 from the Office of Naval Research. The Twin Otter Doppler wind lidar flights were funded by Dr. Steven Mango, chief scientist for the Integrated Program Office of the National Polar Orbiting Environmental Satellite System. Dr. Robert Bluth, director of the Center for Interdisciplinary Remotely Piloted Aircraft Studies provided significant institutional support for the wind lidar missions. Operational COAMPS model output were kindly made available by Dr. Jim Doyle. We thank the four anonymous reviewers for detailed comments and helpful suggestions to improve the paper.

REFERENCES

Bader, D. C., and C. D. Whiteman, 1989: Numerical simulation of cross-valley plume dispersion during the morning transition period. *J. Appl. Meteor.,* **28,** 652–664.

Banta, R. M., 1995: Sea breezes shallow and deep on the California coast. *Mon. Wea. Rev.,* **123,** 3614–3622.

——, L. D. Olivier, and D. H. Levinson, 1993: Evolution of the Monterey Bay sea-breeze layer as observed by pulsed Doppler lidar. *J. Atmos. Sci.,* **50,** 3959–3982.

——, L. S. Darby, P. Kaufmann, D. H. Levinson, and C. J. Zhu, 1999: Wind-flow patterns in the Grand Canyon as revealed by Doppler lidar. *J. Appl. Meteor.,* **38,** 1069–1083.

——, ——, J. D. Fast, J. O. Pinto, C. D. Whiteman, W. J. Shaw, and B. W. Orr, 2004: Nocturnal low-level jet in a mountain basin complex. Part I: Evolution and effects on local flows. *J. Appl. Meteor.,* **43,** 1348–1365.

Bastin, S., P. Drobinski, A. M. Dabas, P. Delville, O. Reitebuch, and C. Werner, 2005: Impact of the Rhone and Durance valleys on sea-breeze circulation in the Marseille area. *Atmos. Res.,* **74,** 303–328.

——, and Coauthors, 2006: On the interaction between sea breeze and summer mistral at the exit of the Rhône Valley. *Mon. Wea. Rev.,* **134,** 1647–1668.

Beardsley, R. C., C. E. Dorman, C. A. Friehe, L. K. Rosenfeld, and C. D. Winant, 1987: Local atmospheric forcing during the coastal ocean dynamics experiment. 1. A description of the marine boundary-layer and atmospheric conditions over a northern California upwelling region. *J. Geophys. Res.,* **92,** 1467–1488.

Bilbro, J. W., and W. W. Vaughan, 1978: Wind field measurement in the nonprecipitous regions surrounding severe storms by an airborne pulsed Doppler lidar system. *Bull. Amer. Meteor. Soc.,* **59,** 1095–1100.

——, and G. D. Emmitt, 1984: Airborne simulation of a satellite based Doppler lidar. *Optical Platforms,* C. L. Wyman, Ed., International Society for Optical Engineering (SPIE Proceedings, Vol. 0493), 321–325.

——, G. Ficht, D. Fitzjarrald, M. Krause, and R. Lee, 1984: Airborne Doppler lidar wind field measurements. *Bull. Amer. Meteor. Soc.,* **65,** 348–359.

Browning, K., and R. Wexler, 1968: The determination of kinematic properties of a wind field using Doppler radar. *J. Appl. Meteor.,* **7,** 105–113.

Carroll, J. J., 1989: Analysis of airborne Doppler lidar measurements of the extended California sea breeze. *J. Atmos. Oceanic Technol.,* **6,** 820–831.

Cui, Z., M. Tjernstrom, and B. Grisogono, 1998: Idealized simulations of atmospheric coastal flow along the central coast of California. *J. Appl. Meteor.,* **37,** 1332–1363.

Darby, L. S., R. M. Banta, and R. A. Pielke, 2002: Comparisons between mesoscale model terrain sensitivity studies and Doppler lidar measurements of the sea breeze at Monterey Bay. *Mon. Wea. Rev.,* **130,** 2813–2838.

De Wekker, S. F. J., D. Steyn, and S. Nyeki, 2004: A comparison of aerosol-layer and convective boundary-layer structure over a mountain range during STAAARTE'97. *Bound.-Layer Meteor.,* **113,** 249–271.

——, ——, J. D. Fast, M. W. Rotach, and S. Zhong, 2005: The performance of RAMS in representing the convective boundary layer structure in a very steep valley. *Environ. Fluid Mech.,* **5,** 35–62.

Drobinski, P., S. Basin, A. Dabas, P. Delville, and O. Reitebuch, 2006: Variability of three-dimensional sea breeze structure in southern France: Observations and evaluation of empirical scaling laws. *Ann. Geophys.,* **24,** 1783–1799.

Fagan, M., 1988: The sea breeze circulation during the Land Sea Breeze Experiment (LASBEX) in central California. M.S.

thesis, Dept. of Meteorology, Naval Postgraduate School, 139 pp. [Available online at http://www.dtic.mil/cgi-bin/GetTRDoc?AD=ADA202196.]

Fosberg, M. A., and M. J. Schroeder, 1966: Marine air penetration in central California. *J. Appl. Meteor.,* **5,** 573–589.

Frehlich, R. G., 2001: Estimation of velocity error for Doppler lidar measurements. *J. Atmos. Oceanic Technol.,* **18,** 1628–1639.

——, 2004: Velocity error for coherent Doppler lidar with pulse accumulation. *J. Atmos. Oceanic Technol.,* **21,** 905–920.

——, and R. Sherman, 2005: Maximum likelihood estimates of vortex parameters from simulated coherent Doppler lidar data. *J. Atmos. Oceanic Technol.,* **22,** 117–130.

Godwin, K. S., S. F. J. De Wekker, and G. D. Emmitt, 2012: Retrieving winds in the surface layer over land using an airborne Doppler lidar. *J. Atmos. Oceanic Technol.,* **29,** 487–499.

Huffaker, R. M., and R. M. Hardesty, 1996: Remote sensing of atmospheric wind velocities using solid-state and CO_2 coherent laser systems. *Proc. IEEE,* **84,** 181–203.

Intrieri, J. M., C. G. Little, W. J. Shaw, R. M. Banta, P. A. Durkee, and R. M. Hardesty, 1990: The Land/Sea Breeze Experiment (LASBEX). *Bull. Amer. Meteor. Soc.,* **71,** 656–664.

Johnson, A., and J. J. O'Brien, 1973: A study of an Oregon sea breeze event. *J. Appl. Meteor.,* **12,** 1267–1283.

Kondo, H., 1990: A numerical experiment on the interaction between sea breeze and valley wind to generate the so-called ''extended sea breeze.'' *J. Meteor. Soc. Japan,* **68,** 435–446.

Lhermitte, R. M., and D. Atlas, 1961: Precipitation motion by pulse Doppler radar. *Proc. Ninth Weather Radar Conf.,* Kansas City, MO, Amer. Meteor. Soc., 218–223.

Post, M. J., and W. D. Neff, 1986: Doppler lidar measurements of winds in a narrow mountain valley. *Bull. Amer. Meteor. Soc.,* **67,** 274–281.

Reitebuch, O., H. Volkert, C. Werner, A. Dabas, P. Delville, P. Drobinski, P. H. Flamant, and E. Richard, 2003: Determination of flow across the Alpine ridge by a combination of airborne Doppler lidar, routine radio-soundings and numerical simulations. *Quart. J. Roy. Meteor. Soc.,* **129,** 715–727.

Rucker, M., R. M. Banta, and D. G. Steyn, 2008: Along-valley structure of daytime thermally driven flows in the Wipp Valley. *J. Appl. Meteor. Climatol.,* **47,** 733–751.

Simpson, J. E., 1994: *Sea Breeze and Local Wind.* Cambridge University Press, 234 pp.

Wagner, A., 1938: Theorie und Beobachtung der periodischen Gebirgswinde (Theory and observation of periodic mountain winds). *Gerlands Beitr. Geophys.,* **52,** 408–449.

Weigel, A. P., F. K. Chow, M. W. Rotach, R. L. Street, and M. Xue, 2006: High-resolution large-eddy simulations of flow in a steep Alpine valley. Part II: Flow structure and heat budgets. *J. Appl. Meteor. Climatol.,* **45,** 87–107.

Weissmann, M. D., F. J. Braun, L. Gantner, G. J. Mayr, S. Rahm, and O. Reitebuch, 2005: The alpine mountain–plain circulation: Airborne Doppler lidar measurements and numerical simulations. *Mon. Wea. Rev.,* **133,** 3095–3109.

Whiteman, C. D., 1990: Observations of thermally developed wind systems in mountainous terrain. *Atmospheric Processes over Complex Terrain, Meteor. Monogr.,* No. 45, Amer. Meteor. Soc., 5–42.

——, 2000: *Mountain Meteorology: Fundamentals and Applications.* Oxford University Press, 355 pp.

Zardi, D., and C. D. Whiteman, 2012: Diurnal mountain wind systems. *Mountain Weather Research and Forecasting,* F. K. Chow, S. F. J. De Wekker, and B. Snyder, Eds., Springer, in press.

Zemba, J., and C. A. Friehe, 1987: The marine atmospheric boundary layer jet in the Coastal Ocean Dynamics Experiment. *J. Geophys. Res.,* **92,** 1489–1496.